

Ricardo Maia Avelino, Tom Van Mele, Philippe Block

Advances in Thrust Network Analysis. Constrained equilibrium assessment of masonry vaulted structures

1. Introduction

The assessment of unreinforced masonry structures requires specialised tools that are not widely available (Tralli, Alessandri, Milani, 2014). Structural modelling of masonry should take into account the unilateral behaviour of the material, related to its high compressive and low tensile strength. Besides, the collapse of masonry structures is usually a result of lack of stability rather than insufficient material strength (Huerta, 2001; Ochsendorf, 2002). For that reason, general-purpose analysis tools which focus on computing the current internal stresses can not be directly applied to the masonry without detailed considerations (Shin *et al.*, 2016). As an alternative, Heyman (1966, 1995) showed that Limit Analysis can be applied to masonry structures given that three assumptions are respected: the material has no tensile strength, infinite compressive strength, and sliding does not occur. Within this framework, the collapse or limit states are searched. In particular, the safe, or lower-bound theorem of limit analysis applies. The theorem states that if at least one admissible stress state can be found, the structure is safe in its current state. When applying the safe theorem to masonry, admissible stress states correspond to compression-only force paths or thrust lines in equilibrium with the applied loads and contained within the geometry of the structure, i.e., between intra- and extrados.

The search for compressive, internal force paths in masonry has been historically applied to arches (Moseley, 1843), sliced domes (Poleni, 1748) and vaults (Ungewitter, 1890), and commonly applied in combination with graphic statics (e.g., Wolfe, 1921). Since these techniques are justified by the safe theorem, they result in a lower-bound (and safe) estimation of the actual capacity of the structure. Currently, this technique is known as Thrust Line Analysis (TLA) and it remains a contemporary tool for the assessment of two-dimensional, or sliced 3D structures (Smars, 2000; Zessin, Lau, Ochsendorf, 2010; Angelillo, Olivieri, DeJong, 2021) and the core of masonry analysis tools (e.g., Limit State: RING, 2021).

Given the independence of major mechanical parameters, lower-bound methods are an important tool for the structural assessment of historic structures, relying exclusively on geometrical data from the intrados and the extrados (Huerta, 2001).

Nevertheless, the extension of lower-bound methods to three dimensions is challenging due to the increased degree of indeterminacy of the three-dimensional equilibrium. The slicing technique (Huerta, 2008) can not explore fully three-dimensional force flows that arise in spatial masonry structures. In recent years, various lower-bound equilibrium formulations have been developed to cope with the assessment of three-dimensional masonry structures. These strategies can be divided into continuous and discrete approaches.

Continuous approaches search for compressive membranes within the geometry of the structure. Heyman (1977) shows that purely applying shell analysis (Calladine, 1983) taking the middle surface of masonry structures often results in tensile membrane stresses, which require an adaptation of the methodology by, e.g., considering sections or slices. Another description of this problem, based on continuum mechanics, takes as variable both: the internal stresses of the membranes and their geometry. The equilibrium equations are solved by assuming a Pucher formulation and considering the potential stress (or Airy) functions to describe the internal distribution of the stresses (Fraternali et al. 2002). With such an approach, the vertical equilibrium is described by a second-order differential equation. To solve the differential equation, different approaches have been developed. In Fraternali (2010) and Angelillo, Babilio, Fortunato (2013), an approximation of the relevant functions is done in polyhedral domains; in Fraddosio, Lepore, Piccioni (2020), a polygonal approximation is used in an equally spaced point grid; in Miki, Igarashi, Block (2015) NURBS surfaces are used and in Baratta, Corbi (2010) analytical solutions are obtained for simple geometries.

On the other hand, discrete methods can be applied avoiding the computation of differential equations offering a flexible formulation that allows considering a wider range of discontinuities in loading, geometry, and boundary conditions. O'Dwyer (1999) proposed a method considering the internal forces in the masonry as a network carrying only compressive, axial forces. Different load cases and flow of forces can be quickly investigated, and the final solution allows to verify and modify the equilibrium by directly changing the internal axial forces at the edges of the network. Nevertheless, in O'Dwyer (1999), no strategy is applied to deal with the indeterminacy of the projected layout of forces.

Following the work of O'Dwyer (1999), Block and Ochsendorf (2007) formalised Thrust Network Analysis (TNA) as a method to compute the internal forces as a network of thrusts based on graphic statics. With such an approach, the spatial equilibrium of networks can be executed interactively by connecting the magnitude of the internal forces with a force diagram analogous to the force polygons in graphic statics (Block, 2009). Further developments of TNA included the framing of the problem as a constrained application of the Force Density Method (Schek, 1973); the introduction of the concept of independent edges, which allow for efficiently searching equilibrium states for thrust networks with a fixed projection (Block, Lachuer, 2014; Van Mele, Block, 2014); and, allowing this equilibrium exploration as a search of admissible solutions through optimisation processes (Block, 2009; Van Mele *et al.*, 2014; Block, Lachauer, 2014). Recent developments extended this framework to determine the level of stability of three-dimensional masonry structures based on the sequential solving of a series of optimisation problems with different objective functions (Maia Avelino *et al.*, 2021) and to consider internal states arising for prescribed foundation settlements (Maia Avelino *et al.*, 2022). This paper gives an overview of the major concepts behind Thrust Network Analysis in the context of masonry assessment. It summarises the recent advances in the method that allow it to be used to search for admissible stress states in three-dimensional masonry structures with generic geometry and output relevant feedback about the level of stability of the structure.

The paper is organised as follows: Section 2 presents the graphic statics based formulation of TNA. Section 3 presents a numerical formulation of TNA suitable for constrained optimisation. Section 4 formulates constrained nonlinear optimisation problems with TNA that are relevant to assess masonry structures. In Section 5, applications to three-dimensional masonry structures are presented. Finally, in Section 6, the conclusion and outlook of the method are described.

2. Graphic statics based approach

This section presents a graphic statics based approach to TNA (2.1) that is analogous to the equilibrium problems in graphic statics. Following, an iterative algorithm to solve the equilibrium in this framework is formulated (2.2).

2.1. On the equilibrium of projected networks

Graphic Statics is a well-known method to find the equilibrium of two-dimensional structures. The relationship between the structure's geometry and its internal forces is described by the reciprocal relation between two diagrams (Culmann, 1875; Wolfe, 1921), the form and force diagrams. The former describes the geometrical configuration of the (axial) internal forces, and the latter represents their equilibrium. A closed polygon in the force diagram represents the equilibrium of a node in the form diagram. Graphic statics offers an intuitive evaluation of the structural equilibrium. It was used as a main structural calculation tool in the late 19th and early 20th century. For masonry analysis, graphic statics offers a straightforward way to find a thrust line within the geometry of a structure. **Figure 1** shows an admissible compressive equilibrium solution, or thrust line (G), found for the semi-circular arch (Λ). The equilibrium in each node of the thrust line relates to the equilibrium of a portion (e.g., a block) subjected to its weight w_i . The force diagram (Γ^*) represents the sum of all closed polygons representing the local equilibria in the nodes of the thrust line. In the force diagram, the length of each segment relates to the force carried in the corresponding segment in the thrust line. By modifying the force diagram, e.g., by moving the pole point (o) and choosing the coordinates of one of the nodes of the form diagram, the internal (and reaction) forces and the shape of the thrust line can be changed, and different equilibrium solutions explored.

The graphic formulation of TNA offers a 2.5D extension of 2D graphic statics (Block, Ochsendorf, 2007). In this formulation, the loading case is assumed to be parallel, which often occurs in masonry structures, e.g., the gravity loads and horizontal force multipliers. When all loads are parallel, the spatial thrust network can be projected onto a plane perpendicular to the loads resulting in a two-dimensional graphic statics problem in which the applied loads vanish.

For the gravity loading case, the projection of the thrust network (G) results in the planar form diagram (Γ) for which the horizontal equilibrium can be described graphically with the construction of the force diagram (Γ^*), respecting the same well-known two-dimensional graphic statics procedures. In this case, Γ^* represents the equilibrium of the horizontal components of the forces, i.e., the (horizontal) thrusts of G . If we formalise these concepts in TNA, the horizontal equilibrium is verified when the diagrams are reciprocal, which implies that:

- All corresponding edges in the form and force diagrams are parallel.
- The length of an edge in the force diagram is proportional to the axial force, carried by its corresponding edge in the form diagram.
- Each node in the form diagram is represented by a closed polygon in the force diagram.

Figure 2 shows a thrust network (G) whose horizontal equilibrium can be described graphically by their reciprocal form and the force diagrams. This thrust network models a possible distribution of the internal forces in a masonry cap (Λ), i.e., each vertically applied load relates to the weight of a portion (e.g., a block) of the structure and the position of the vertices match the vertical projection of the centroids. The thrust network (G) is admissible as all forces are compressive and the network fits within the geometry of Λ . As in the 2D problem, modifying the geometry of the force diagram while respecting reciprocity with the form diagram leads to different equilibrium solutions for that form diagram.

The form diagram represents the horizontal layout of the thrusts, i.e., and a map of the force flow within the structure. In the context of masonry assessment, the form diagram is chosen (or generated) by the engineer based on intuition or experience on likely force paths within the structure, usually following its main geometric features, such as principal curvature or creases.

With this approach, the equilibrium of a node in G can be divided into horizontal and vertical components. For node i , shown in **figure 3**, the horizontal and vertical equilibria are described by the following equations:

$$\begin{aligned} f_{ji}^H + f_{ki}^H + f_{li}^H &= 0, \\ f_{ji}^V + f_{ki}^V + f_{li}^V &= p_i, \end{aligned} \quad [1.1-1.2]$$

where f_{ji}^H and f_{ji}^V describe the horizontal and vertical components of an edge's (axial) force connecting nodes j and i , and p_i is the load lumped in the node.

With the decoupling of horizontal and vertical equilibrium, there are multiple ways in which these equations can be treated and solved. In the following section, we discuss an interactive, graphic way to solve the horizontal equilibrium in Equation 1.1.

2.2. Interactive graphic equilibrium

We introduce the following nomenclature, the form diagram Γ is composed of m edges and n nodes with planar coordinates stored in the vectors \mathbf{x} , \mathbf{y} . Each edge \mathbf{e}_{ij} connects vertices i and j with a length l_{ij} and force f_{ij} . The elements of the force diagram Γ^* are marked by an asterisk (*), such that the diagram has m^* edges and n^* nodes. Each edge \mathbf{e}_{ij}^* of the force diagram has length l_{ij}^* . The thrust network (G) corresponds to the vertical lift of Γ , where the vertical nodal coordinates are stored in the vector \mathbf{z} .

To find reciprocal form and force diagrams, a parallelisation algorithm has been proposed in Rippmann, Lachauer, Block (2012) and is described herein. It starts with a form diagram and its dual diagram, so not yet a force diagram representing a possible equilibrium for it, and updates the vertex positions of both diagrams to match the target orientation of its corresponding edges, such that at the end of the process the diagrams are reciprocal. To obtain a force diagram, the algorithm starts from the centroidal dual topology of the form diagram. Details about the automatic generation of the centroidal dual topology are given in Rippmann, Lachauer, Block (2012).

To find an initial state of equilibrium, target vectors \mathbf{t}_{ij} are imposed to the edges of the form and force diagrams to parallelise the corresponding edges. Not only the force diagram can be aligned with the original form diagram but a weighting factor $\gamma = \{0, \dots, 1\}$ can be introduced, which increases or decreases the influence of the form diagram to define the target directions to be used in the parallelisation. The target vector \mathbf{t}_{ij} for each pair of corresponding edges \mathbf{e}_{ij} and \mathbf{e}_{ij}^* is then computed as follows:

$$\mathbf{t}_{ij} = \gamma * \hat{\mathbf{e}}_{ij} + (1 - \gamma) \hat{\mathbf{e}}_{ij}^*, \text{ with } 0 \leq \gamma \leq 1, \quad [2]$$

where $\hat{\mathbf{e}}_{ij}$ and $\hat{\mathbf{e}}_{ij}^*$ are the normalised directions of edges \mathbf{e}_{ij} and \mathbf{e}_{ij}^* .

With the target direction and vectors, the solver iterates over all nodes of the form and force diagrams and calculates an updated vertex positions \mathbf{P}_i and/or \mathbf{P}_i^* . The procedure is applied analogously to both diagrams and is described here to update the force diagram.

Let E_i represent the group of edges \mathbf{e}_{ij}^* connected to a vertex \mathbf{v}_i^* of the force diagram with target vector \mathbf{t}_{ij} computed for a given Γ , and target length l_{ij}^* . The updated position \mathbf{P}_i^* of this node is computed by:

$$\mathbf{P}_i^* = \frac{\sum_{j \in E_i} (\mathbf{v}_i^* + l_{ij}^* * \hat{\mathbf{t}}_{ij})}{n(E_i)}, \quad [3]$$

where $n(E_i)$ is the number of neighbors of vertex \mathbf{v}_i^* .

This iterative approach is applied to all nodes of the form and force diagrams until the stopping criteria is reached, i.e. corresponding edges have the same direction within a chosen maximum deviation angle α_{MAX} . This interactive approach also indirectly imposes that the networks are subjected to compressive-only forces as for these cases Γ^* must be composed of non-overlapping, convex spaces (Rippmann, Lachauer, Block, 2012).

With this algorithm, interactively exploring equilibrium interactively is possible by stretching or moving nodes in the force diagram, after which the iterative solver finds the new reciprocal state as close as possible to the modification considering the weighting factor γ .

Once horizontal equilibrium is achieved, the horizontal forces (f_{ji}^H) in the form diagram are taken as the lengths of the force diagram (l_{ji}^*) multiplied by a scaling factor $1/r$:

$$f_{ji}^H = \frac{1}{r} * l_{ji}^* . \tag{4}$$

Therefore, by stretching members of the force diagram, the force lengths l_{ij}^* are increased and so are the forces in the corresponding edges of the form diagram f_{ji}^H . **Figure 4** shows four different equilibria obtained by re-distributing the horizontal thrusts in an orthogonal grid supported along its boundary. An equally distributed configuration is shown in **figure 4a**. In **figures 4b-d**, the forces are increased in the edges highlighted, attracting forces that result in shallow arches, or creases in the thrust networks (G). Following the computation of a possible horizontal equilibrium through parallelisation, the vertical equilibrium is solved as a separate step. It corresponds to performing a lifting of the horizontally equilibrated network. Assuming the obtained horizontal forces (Equation 5), the vertical equilibrium (1.2) can be rewritten as:

$$f_{ji}^H * \frac{(z_i - z_j)}{l_{ij}^H} + f_{ki}^H * \frac{(z_i - z_k)}{l_{kj}^H} + f_{li}^H * \frac{(z_i - z_l)}{l_{li}^H} = p_i , \tag{5}$$

which, after substituting the horizontal forces (4), can be rearranged as:

$$\left(\frac{l_{ji}^*}{l_{ji}^H} + \frac{l_{ki}^*}{l_{ki}^H} + \frac{l_{li}^*}{l_{li}^H} \right) z_i - \left(\frac{l_{ji}^*}{l_{ji}^H} \right) z_j - \left(\frac{l_{ki}^*}{l_{ki}^H} \right) z_k - \left(\frac{l_{li}^*}{l_{li}^H} \right) z_l = p_i * r , \tag{6}$$

which is a linear function in terms of the height of the nodes (z_i) and the scaling factor. This scaling factor allows for searching for globally deeper or shallower thrust networks for a given horizontal equilibrium distribution, as shown in **figure 5**.

This framework has been applied to the design of new compressive vaulted structures. Manually stretching and moving nodes in the force diagrams bring intuitive and direct visual feedback to the horizontal distribution of forces and resulting thrust networks.

To make this intuitive forward TNA-based form-finding approach available, RhinoVault, a plug-in for the CAD software Rhinoceros, was developed (Rippmann, Lachauer, Block, 2012; Rippmann, 2016). Also, a Python-based code implementation of TNA has been made available as the *compas_tna* package (Van Mele, 2020), built on the open-source computational framework COMPAS (Van Mele *et al.*, 2017). Recently, RhinoVault 2, an implementation of the TNA package as a robust updated version of RhinoVault, has been released (Block Research Group, 2020).

However, when it comes to masonry assessment, the search for admissible networks needs to be automated since it relates to finding particular solutions that are contained within (usually tight) upper and lower geometric bounds. Manual manipulation of the diagrams to achieve such particular geometric solutions is tedious, if not impossible, so this search must be executed by means of optimisation. To cope with this automation, a numerical formulation of TNA is proposed based on Block (2019) and Block, Lachauer (2014), which will be described in the following section.

3. Numerical TNA formulation

A more robust numerical control of the equilibrium can be achieved by relating the use of form and force diagrams in TNA to the equilibrium of general networks through the use of the force density method (FDM) (Schek, 1974). This is shown in detail in Block (2009) and Block, Lachauer (2014) and will be summarised in Section 3.1. More specifically, TNA can be seen as a special case of FDM in which the horizontal projection of the equilibrium solutions, i.e. the form diagram, is constrained to remain fixed.

To restrict the problem to a fixed planar diagram, the degrees of freedom in the pattern must be identified, adding constraints to the full set of force densities, as described in Section 3.2.

3.1. Constrained force density formulation

To rewrite Equation 6 in matrix format, we introduce the connectivity matrix \mathbf{C} [$m \times n$], which describes the connectivity of an oriented network:

$$\mathbf{C} = \begin{cases} 1 & \text{if vertex } i \text{ is the head of edge } j \\ -1 & \text{if vertex } i \text{ is the tail of edge } j \\ 0 & \text{otherwise} \end{cases} \quad [7]$$

As shown in Equation 6, considering the quotient of the force and the length of the edge in the network linearises the vertical nodal position of the networks. This quotient is also known as the force density of an edge q_{ij} , defined and connected to the initial variables as follows:

$$q_{ij} = \frac{f_{ij}}{l_{ij}} = \frac{f_{ij}^H}{l_{ij}^H} = \frac{1}{r} * \frac{l_{ij}^{H*}}{l_{ij}^H} \quad [8]$$

Using the general FDM description, external loads can be applied to any direction through the vectors $\mathbf{p}_x, \mathbf{p}_y, \mathbf{p}_z$ [$n \times 1$], which are partitioned in $\mathbf{p}_{x,i}$ and $\mathbf{p}_{x,b}$ referring to the n_i free and n_b fixed, or constrained nodes in the network (analogously in y - and z - directions). Similarly, the connectivity matrix can be sliced in \mathbf{C}_i [$m \times n_i$] and \mathbf{C}_b [$m \times n_b$]. Using this definition and introducing the coordinate difference matrices $\mathbf{U} = \text{diag}(\mathbf{C}_i \mathbf{x}), \mathbf{V} = \text{diag}(\mathbf{C}_i \mathbf{y}), \mathbf{W} = \text{diag}(\mathbf{C}_i \mathbf{z})$ [$m \times m$] the equilibrium equations in the free nodes can be rewritten for x -, y -, and z - direction as:

$$\begin{aligned} \mathbf{C}_i^T \mathbf{U} \mathbf{q} &= \mathbf{p}_{x,i}, \\ \mathbf{C}_i^T \mathbf{V} \mathbf{q} &= \mathbf{p}_{y,i}, \\ \mathbf{C}_i^T \mathbf{W} \mathbf{q} &= \mathbf{p}_{z,i}. \end{aligned} \quad [9.1-9.3]$$

Finally, the coordinates of a network with given applied loads can be computed in terms of the positions of the fixed vertices $\mathbf{x}_b, \mathbf{y}_b, \mathbf{z}_b$ [$n_b \times 1$] and of the force densities in all edges \mathbf{q} .

$$\begin{aligned} \mathbf{x}_i &= (\mathbf{C}_i^T \mathbf{Q} \mathbf{C}_i)^{-1} (\mathbf{p}_{x,i} - \mathbf{C}_b^T \mathbf{Q} \mathbf{C}_b \mathbf{x}_b), \\ \mathbf{y}_i &= (\mathbf{C}_i^T \mathbf{Q} \mathbf{C}_i)^{-1} (\mathbf{p}_{y,i} - \mathbf{C}_b^T \mathbf{Q} \mathbf{C}_b \mathbf{y}_b), \\ \mathbf{z}_i &= (\mathbf{C}_i^T \mathbf{Q} \mathbf{C}_i)^{-1} (\mathbf{p}_{z,i} - \mathbf{C}_b^T \mathbf{Q} \mathbf{C}_b \mathbf{z}_b), \end{aligned} \quad [10.1-10.3]$$

where $\mathbf{Q} = \text{diag}(\mathbf{q})$.

Therefore, by using this general approach, all coordinates in a network can be controlled by modifying the force densities and the positions of the support vertices of the network.

However, controlling the specific position of the network using all \mathbf{q} as parameters is a hard problem. The clarity imposed by the definition of the form diagram is lost in such general application; particular features such as creases, crack lines, and load-point applications can no longer be considered. Furthermore, dense diagrams might easily present more than 1000 edges, increasing the number of parameters of an optimisation. In the next section, a strategy for decoupling the horizontal and vertical equilibrium is presented and explored by defining the degrees of freedom of form diagrams fixed in plan.

3.2. Degrees of freedom of a network with fixed projection

To reduce the degrees of freedom of Equation 10 and to keep the form diagram fixed, a linear relationship is introduced to the force densities in the network. Assuming that \mathbf{x} , \mathbf{y} and \mathbf{U} , \mathbf{V} are known, the horizontal equilibrium equations 9.1 and 9.2 can be combined introducing the horizontal equilibrium matrix \mathbf{E} [$2n \times m$]. Similarly, the applied horizontal external forces are combined in the vector $\mathbf{p}_{h,i}$ resulting in the following expression:

$$\mathbf{E}\mathbf{q} = \mathbf{p}_{h,i}, \quad \text{with: } \mathbf{E} = \begin{bmatrix} \mathbf{C}_i^T \mathbf{U} \\ \mathbf{C}_i^T \mathbf{V} \end{bmatrix}, \mathbf{p}_{h,i} = \begin{bmatrix} \mathbf{p}_{x,i} \\ \mathbf{p}_{y,i} \end{bmatrix}. \quad [11]$$

Finding a set of force densities satisfying Equation 11 means finding a distribution of horizontal forces in the fixed pattern. Furthermore, if we constrain all force densities to be negative, this solution will be compression only (Section 4).

The number of force densities that can be chosen freely in Equation 11 corresponds to the number of degrees of freedom (DOFs) of the fixed form diagram. This number is equal to the rank deficiency of the matrix \mathbf{E} (Van Mele *et al.*, 2014). These are known as independent force densities \mathbf{q}_{id} and can be found through sequential singular-value decomposition as shown in Maia Avelino *et al.* (2021). Once the independent edges are determined, the set of dependent force densities can be computed with:

$$\mathbf{q}_d = -\mathbf{E}_d^\dagger (\mathbf{E}_i \mathbf{q}_{id} - \mathbf{p}_{h,i}), \quad [12]$$

where \mathbf{E}_d and \mathbf{E}_i are slices of \mathbf{E} related to the dependent and independent edges, respectively, and \mathbf{E}_d^\dagger corresponds to the generalised inverse or Moore-Penrose pseudoinverse of \mathbf{E}_d . Once \mathbf{q}_d is computed from \mathbf{q}_{id} , the vector of force densities \mathbf{q} in the system is retrieved through the linear transformation

$$\mathbf{q} = \mathbf{B}\mathbf{q}_{id} + \mathbf{d}, \quad \text{with: } \mathbf{B} = \begin{bmatrix} -\mathbf{E}_d^\dagger \mathbf{E}_i \\ \mathbf{I}_k \end{bmatrix}, \mathbf{d} = \begin{bmatrix} \mathbf{E}_d^\dagger \mathbf{p}_{h,i} \\ \mathbf{0} \end{bmatrix} \quad [13]$$

where \mathbf{I}_k is the identity matrix of size k . After such variable reduction, the vertical coordinates of the network are now function of \mathbf{q}_{id} and \mathbf{z}_b :

$$\mathbf{z}_i(\mathbf{q}_{id}, \mathbf{z}_b) = (\mathbf{C}_i^T \mathbf{Q} \mathbf{C}_i)^{-1} (\mathbf{p}_{z,i} - \mathbf{C}_b^T \mathbf{Q} \mathbf{C}_b \mathbf{z}_b) \quad [14]$$

An initial approximation of the vertical loads ($\mathbf{p}_{z,i}$) can be computed at the beginning of the process. After the definition of the form diagram in plan, projected tributary areas per vertex can be directly obtained from it.

It is worth noting that this formulation can cope with horizontal external loads in the vector $\mathbf{p}_{h,i}$ as long as the form diagram is able to transfer the loads to the supports, which requires that the rank of \mathbf{E} is not increased by concatenating $\mathbf{p}_{h,i}$ as a column (Bruggi, 2020).

For the cases where no horizontal loads are applied, a force diagram can always be retrieved from the in-equilibrium force densities (Van Mele *et al.* 2012). In fact, the degrees of freedom of the pattern corresponds to the possible modifications in the force diagram that will preserve the orientations of the edges of the form diagram (Block, 2019; Block, Lachauer, 2014). **Figure 6** shows such manipulations for the orthogonal form diagram used in the previous examples [fig. 4] with one set of independent edges highlighted in blue. For this diagram, the selection of the independent edges and their effects on the resulting internal force pattern is trivial: each continuous line must have one independent edge and thus an independent thrust value. **Figure 6** shows the modifications necessary to obtain Γ_1^* [fig. 4b] and Γ_2^* [fig. 4c], where the (horizontal) force in the independent edge controlling the central continuous arch in the structure is increased by a factor of 4.0.

In general cases, especially for triangulated patterns, finding these independent edges and understanding their effect in the global horizontal equilibrium is not trivial. **Figure 7** shows a set of independent edges for the corner-supported form diagram Γ . Next to it, an individual increase in

the force magnitude for each independent edge is applied, and the force diagram Γ_i^* and thrust network G_i obtained are depicted. The infinite combination of the individual effect of all independent edge represent the possible (horizontal) equilibrium states for the form diagram Γ , resulting in different thrust networks G .

The main advantage of the numerical formulation presented in this section is that the problem is now reduced in terms of variables - the independent edges (\mathbf{q}_{id}) and the heights of the fixed vertices (\mathbf{z}_b) - which is especially suitable for the optimisation algorithms presented in Section 4. In this formulation, the horizontal equilibrium in Equation 13 is decoupled from the vertical but they are computed simultaneously. Therefore, all possible horizontal equilibria are considered when searching for different networks within geometric bounds. As a consequence, the presented numerical approach enables to explore the full equilibrium space of the problem.

4. Searching for admissible stress states

This section presents the latest research on TNA in which the problem of searching for admissible stress states is encoded in a nonlinear constrained optimisation process. The overall nonlinear programming (NLP) problem and different objective functions are discussed in Section 4.1. In Section 4.2, a method to compute the level of stability of a masonry vault is presented.

4.1. A nonlinear optimisation framework

Finding networks with specific geometric configurations is a hard numerical problem because the heights of the network are nonlinear with respect to the independent force densities (\mathbf{q}_{id}) per Equation 14. The general problem that needs to be solved for the assessment of masonry structures, is presented below for a generic objective function f_{obj} :

$$\min_{\mathbf{q}_{id}, \mathbf{z}_b} f_{obj}(\mathbf{q}_{id}, \mathbf{z}_b), \quad [15.1]$$

$$\text{s. t.} \quad \mathbf{q} = \mathbf{B}\mathbf{q}_{id} + \mathbf{d}, \quad [15.2]$$

$$q_j \leq 0, \quad \text{for } j = \{1, 2, \dots, m\}, \quad [15.3]$$

$$z_i^{LB} \leq z_i \leq z_i^{UB}, \quad \text{for } i = \{1, 2, \dots, n\}, \quad [15.4]$$

in which the variables are the independent force densities \mathbf{q}_{id} and the heights of the supports \mathbf{z}_b . The force densities in all edges are computed per Equation 15.2. Equation 15.3 imposes the compression-only constraints to all force densities of the network, which are constrained to be negative. Equation 15.4 imposes that the vertical heights of the network are contained within the envelope of the masonry described through the upper and lower bound heights, z_i^{UB} and z_i^{LB} , at each vertex i . Additional constraints and variables can be coupled to this modular optimisation framework.

The optimisation problem described in Equation 15 can be solved with general NLP solvers, such as interior point optimisation (IPOPT) (Wächter, Biegler, 2006), Method of moving asymptotes (MMA) (Svanberg, 1987), and Sequential Least Squares Programming (SLSQP) (Kraft, 1988). The derivatives and gradients have been computed analytically in (Van Mele *et al.*, 2014; Bruggi, 2020; Maia Avelino *et al.*, 2021).

Different works in the literature have assumed distinct objective functions to the general optimisation framework. In Block, Lachauer (2014) and Van Mele *et al.* (2014), the objective function selected is the “best fit”. This objective minimises the vertical least-square distances of the network’s vertices to given target heights. In these works, the explicit constraints on the bounds (Equation 15.4) are not considered.

In subsequent works (Bruggi, 2020; Maia Avelino *et al.*, 2021), the bounds on intrados and extrados are explicitly considered and multiple objective functions are considered. In Maia Avelino *et al.* (2021), three objective functions are considered: minimising and maximising the horizontal reactions and offsetting the starting envelope to find the minimum thickness for the structure. These objective functions are used to assess the level of stability through the construction of the stability domain, as will be explained in Section 4.2.

It is worth noting that in Block and Lachauer (2014), Bruggi (2020) and Maia Avelino *et al.* (2021) no assumption is made on the distribution of the horizontal forces of the network. The horizontal equilibrium is computed automatically, so without the need to enforce bounds to the thrusts as in O’Dwyer (1999) or Marmo, Rossati (2017).

Most recently, in Maia Avelino *et al.* (2022), the complementary energy of the network is minimised for a given vector of virtual displacements applied to the supports, which is adequate to model the behaviour of masonry structures subjected to differential foundation settlements.

Further objective functions are also possible, e.g., maximising a horizontal multiplier of the applied loads can be incorporated into the present workflow. This is the static equivalent for computing a horizontal action such as an earthquake, which can be simplified to a horizontal load equal to a fraction of the structure' self-weight (Milani *et al.*, 2016; Nodargi, Bisegna, 2021).

Figure 8 illustrates different objective functions relevant for the assessment of vaulted masonry structures applied to a semi-circular arch, these that can be coupled to the optimisation problem in Equation 15. **Table 1** shows the objective function for each case and a description. This list is non-exhaustive and further work might expand it including new relevant objective function implementations.

Objective Function		f_{obj}	Description
a	Minimise horizontal thrust	$\sum_{n_b} \sqrt{R_{x,i}^2 + R_{y,i}^2}$	Minimises the horizontal component of the emerging reactions $(R_{x,i}, R_{y,i})$.
b	Maximise horizontal thrust	$\sum_{n_b} -\sqrt{R_{x,i}^2 + R_{y,i}^2}$	Maximises the horizontal component of the emerging reactions $(R_{x,i}, R_{y,i})$.
c	Minimise thickness	t	Minimises the structural thickness ($t > 0$) computed orthogonally to the masonry's middle surface.
d	Best-fit	$\sum_n (z_i - z_i^t)^2$	Minimises the least-square vertical distance of the network to a target surface with heights z_i^t .
e	Minimise complementary energy	$\sum_{n_b} \mathbf{R}_i \cdot \boldsymbol{\phi}_i$	Minimises the complementary energy defined as sum of the dot product of the reactions $(\mathbf{R}_i \in \mathbb{R}^3)$ times the foundation displacements $(\boldsymbol{\phi}_i \in \mathbb{R}^3)$.
f	Maximise horizontal multiplier	λ	Maximises the horizontal load multiplier ($\lambda \geq 0$) which applies a horizontal load proportional to the masonry's selfweight.

Table 1: Different objective functions that can be implemented in TNA.

4.2. Computing the level of stability

In a practical assessment scenario, assessing the level of stability of the structure is pressing. It implies answering how far the structure is from the collapse state, or how stable it is in its current configuration. However, finding one admissible stress state (as in the dome cap of **figure 2**) informs that the structure in its configuration is safe. Still, it does not provide information about the level of stability.

Furthermore, most of the optimisation objectives described in Table 1 alone can not give a quantity indicating the safety, i.e. the level of stability. A measure to compute the closeness to collapse on masonry structures was proposed in Heyman (1968, 1995) as the geometric safety factor (GSF). The GSF is defined as the ratio of the current thickness of the structure and its minimum thickness, i.e. the minimum thickness of the structure for which it is still stable. In Maia Avelino *et al.* (2021), the minimisation of the thickness is presented for analytic and non-analytic masonry geometries, resulting in the value of the GSF.

A more consistent measure of the level of stability is provided by defining the size of the space of admissible solutions. A reasonable measure of this domain is represented by its extreme (minimum and maximum) thrusts. For all but the limit state, the minimum and maximum thrust correspond to different stress states and have distinct (horizontal) thrust values. However, at the limit state, minimum and maximum thrust coincide. In Maia Avelino, *et al.* (2021), the stability domain is traced for reduced values of thickness, until the point of collapse. Understanding how the stability domain changes as a function of the thickness gives a direct measure of the robustness of the structure from its initial state, until the collapse state. This robustness can be associated with the structure's capacity to carry additional imposed loads or undergo external settlements.

By combining these two measures, a picture of the stability and robustness of the structure can be drawn, which is in accordance with the lower-bound, or safe theorem, in which the stability domain is approximated by the interior, i.e., by the safe side.

5. Applications

In this section, recent results obtained using Thrust Network Analysis are compiled to showcase the wide range of applications of the method to relevant masonry assessment problems. Section 5.1 shows the application of TNA for the computation of the stability domain and geometric safety factor of a hemispherical dome. Section 5.2 shows how a similar approach can be applied to general vaults, comparing different assumptions on force flows by evaluating different form diagrams. Finally, Section 5.3 shows an application of TNA in combination with an energy criteria, which might be used for the inverse analysis of structures subjected to foundation displacements.

5.1. Assessment of a hemispherical dome

The first example considers a hemispheric dome which will be described by the ratio between its thickness and its central radius t/R_c . The dome is assumed to have an initial thickness $t_0/R_c=0.10$ as is depicted in **figure 9a**. We assume the form diagram depicted in **figure 9b** to perform the TNA analysis. This diagram is composed of 20 hoops that are equally spaced in plan and 16 meridian segments that link the outer perimeter of the pattern to the centre. The final diagram is composed of 640 edges, for which a possible set of 33 independents are highlighted in blue in **figure 9b**. The shape of the thrust network is, therefore, a parameter of the 33 independent force densities and 16 vertical support heights, resulting in a total of 49 variables.

To study the stability of this dome, first, a minimum-thickness analysis is performed by computing the optimisation problem of Equation 15, having as objective function the direct minimisation of the thickness of the dome (Table 1c). The equilibrium result obtained is depicted in **figure 9c-9d** resulting in a $t_{MIN}/R_c=0.041$. In **figure 9c**, the edges of the thrust network that carry zero force are not shown, and the edges carrying (compressive) forces have their thickness scaled proportional to the forces carried. Points touching intrados and extrados are highlighted in blue and green, respectively.

A qualitative description of the minimum thickness solution shows that on the central part of the dome a bi-axial compressive cap is observed and a uniaxial stress state forms towards the supports, where the hoop forces vanish. Such internal force distribution is aligned with the “orange slice” mechanism proposed in Heyman (1988) for an outward (passive) radial displacement of the supports. The minimum thickness obtained in the TNA analysis is also in accordance with the theoretical minimum thickness of $(t_{MIN}/R_c)_{theory}= 0.042$, computed in Heyman (1988), presenting an error of less than 2%.

Comparing this minimum thickness to the initial dome thickness, the GSF of the dome can be calculated as 2.44, which allows one to conclude that a hemispherical dome with a given thickness over radius $t_0/R_c = 0.10$ is safe under its self-weight.

Further analysis of the stability of the dome can be provided by plotting the stability domain for the initial thickness $t_0/R_c = 0.10$. This is done by successively computing the minimum and maximum thrusts of the dome for decreasing offset thicknesses.

Figure 10 shows the result of such a process, where the values of minimum and maximum thrust, normalised by the dome's weight (T/W), are plotted as percentages in blue and red, respectively. The stability domain corresponds to the area between the two curves, highlighted in grey. In this area, one can find all admissible stress states of the problem for the given starting geometry and chosen form diagram. This stability domain is nonlinear and shrinks parabolically towards the limit state, giving an idea of the drop of stability for reduced values of thickness.

Points A, B, and C can be extracted from the stability domain; they represent the maximum and minimum thrusts in the original state and the point with minimal thickness (limit state). The maximum and minimum thrust-over-weight is equal to 62.6% and 19.9% while the value of thrust over weight for the limit state is 24.3%. Further discussion on this example and an extended mesh sensitivity study are available in Maia Avelino *et al.* (2021).

5.2. Assessment of a gothic masonry vault

The second example deals with a Gothic vault constructed parametrically from the cross-sectional parameters defined in **figure 11a**. The parameters assumed are the base length (l_0), central radius (R), springing angle (β), the thickness of the vault (t) and the effective span (s). The thickness of the vault is computed orthogonally to the middle surface, and the effective span is obtained from the ratio R/l_0 and the springing angle β .

The geometry of a vault obtained with $R/l_0 = 0.71$, $t/s = 0.05$, and $\beta = 20^\circ$ is depicted in **figure 11b** and will be used in this analysis.

Unlike the first dome example, suggesting a layout for the forces in the vault is not straightforward. For that reason, the three patterns of **figure 12** are considered. These patterns represent different force-flow assumptions within the structure. Pattern (a) is named orthogonal diagram and presents orthogonal segments that converge to main diagonals that transfer the forces to the supports of the vault. Pattern (b) is the fan-like diagram, which directly connects the supports of the structure and its central portion (spandrel). In pattern (c), diagonals are added to pattern (a), allowing additional possible paths to the supports, and the unsupported boundaries are curved inwards.

For all patterns, only the four corners are set as supports, and the independent edges are highlighted in blue [**fig. 12**].

The self-weight of the vault is lumped into the vertices of the pattern following a 3D tributary area calculation based on the projection of the patterns onto the middle surface of the vault multiplied by the thickness. For each form diagram, the minimum thickness and the stability domain of the Gothic vault are computed. The results are depicted in **figure 13**.

From the analysis of **figure 13**, we can see that the three different diagrams give a slightly different evaluation of the level of stability for the vault. The curved diagram [**fig. 12c**] yields the minimum thickness, i.e., the one resulting in the highest GSF of 2.5 and minimum thickness-over-span of 0.02. The three-dimensional minimum thickness solution obtained with this diagram is depicted in **figure 13**. The orthogonal and the fan-like diagrams result in reduced GSFs, which are (coincidentally) the same for both diagrams and equal to 2.1 (minimum thickness-over-span of 0.026). Therefore, by studying the stability of this specific Gothic vault conducting an analysis with both diagrams would be (equally) too conservative. Yet, the minimum overall thrust of the structure is obtained with the orthogonal pattern, which can be associated with the preferred flow of forces for an outward (opening) displacement of the vault.

In conclusion, when assessing structures with TNA, the analysis of multiple diagrams is crucial. Indeed, the structure can assume different force flows for different states (i.e., extreme thrusts and minimum thickness). This reflects how masonry structures are able to adapt to different support displacements, which induce different internal stress states, as also referred to by other authors as an elastic behaviour (Huerta, 2001). As the solutions are always safe, i.e., correspond to a lower-bound of the collapse state, the analysis can be performed with multiple diagrams, and the real domain of stability of the vault corresponds to the convex envelope of the multiple distinct domains obtained with different diagrams. A complete parametric study of this problem is available in Maia Avelino *et al.* (2021b).

5.3. Compatible stress states for given foundation displacements

The last example shows how TNA can be linked with an energy criteria allowing to compute compatible stress states for a given set of (virtual) foundation displacements. The example considered is the same hemispheric dome of Section 5.1 with thickness over central ratio $t/R_c = 0.10$. As shown in Section 5.1, the dome is safe under its self-weight.

However, in practical assessment scenarios, cracks are often observed in

supposedly safe structures, which require a proper analysis to avoid unnecessary closures and interventions (Iannuzzo *et al.*, 2021). These cracks appear as a consequence of the unilateral (compression-only) nature of unreinforced masonry structures and arise in most cases due to foundation displacements. Measuring the exact magnitude or even identifying where the displacement is taking place is challenging. An energy criteria can be used to perform an inverse analysis that associates the observed crack pattern in the structure with an assumption of the actual displacements that occur at the base, which can be done by minimising the structure's complementary energy (Iannuzzo *et al.*, 2021).

The complementary energy of the structure corresponds to the work of the reaction forces once a given displacement is imposed to the supports of the structure. By computing the minimum complementary energy of the structure subjected to a given set of displacements, a stress state can be found compatible with the given foundation displacement, which reveals the locations where cracks are most likely to form.

The optimisation framework in Equation 15 can be modified to perform such analysis by assuming as objective function the complementary energy for a given foundation displacement map (Table 1e). The foundation displacement map imposed in **figure 14a** corresponds to the spreading of the supports of a dome in two halves. The solution is depicted in **figures 14b-d**.

The solution obtained shows that for the spreading of the dome in two halves, the forces tend to accumulate in the Section B-B, in the middle portion orthogonal to the movement. In this Section, the force distribution assumes a maximum thrust behaviour, as can be seen in **figure 14c**. Along Section A-A, parallel to the movement, there's a clear depression in the centre of the dome [**fig. 14d**], suggesting the two halves tilting inwards and imposing higher pressure onto the arch along Section B-B. Similarly to the observation for the minimum-thickness case in Section 5.1, a uniaxial stress state forms towards the base of the dome, suggesting meridional cracks, while the bi-axial cap remains in place, now following the tilting provoked by the support movement [**fig. 14c**].

In a practical scenario, the crack pattern suggested by the analysis can be compared to the cracks observed. The TNA model can then be adjusted so additional analyses are performed to investigate the most likely reason for observed cracks to form.

6. Conclusions

In this overview paper, the formulation of Thrust Network Analysis (TNA) is revisited, focusing on its application to assessing unreinforced vaulted masonry structures. TNA offers a fast and flexible methodology to compute lower-bound admissible equilibrium solutions for a given masonry envelope. The internal forces are discretised and lumped in a network with axial-only forces along the edges and external loads and supports assigned to the vertices.

First, a graphic formulation of the method is presented for which the connections with ancient graphic statics methods is highlighted. Form and force diagrams are introduced, the former representing the projection onto the plane of the internal axial forces and the second representing the horizontal equilibrium of the former. This graphic-statics-based TNA framework is particularly relevant for interactive funicular form exploration in a forward design process.

Then, a numerical and more robust formulation is presented, which allows framing TNA in optimisation processes necessary for its application in a masonry assessment context.

The fixed form diagram offers the analyst additional control to model major geometrical features and/or structural discontinuities, such as creases, cracks or point loads of the masonry structure to assess.

Recent advances in the method are presented in which multiple objective functions are possible. These focused on framing the method as a tool for masonry assessment by providing a consistent measure of the level of stability represented by the computation of the GSF and the stability domain. The latter is traced by computing the extreme (minimum and maximum) thrust values of the structure ranging from its current state to the minimum-thickness state. Further developments coupled TNA with an energy criteria, which allow the study of compatible admissible networks for given foundation displacements.

Finally, the intense recent activity on lower-bound equilibrium methods, including continuous and discrete methods, such as TNA, suggests that more research will arise in searching for admissible stress states in masonry vaulted structures. Multiple challenges and open questions remain, such as how to overcome the specificity of the form diagram and provide engineers with adapted or automatically generated diagrams for the analysis.

Future work points to connecting the admissible solutions to energy-based methods and comparing them with general, rigid-block-based three-dimensional tools.

Moreover, open-source computational tools are being developed based on TNA and other lower-bound methods, which will increase the number of assessment tools available, benefiting other researchers and practising engineers in the field of structural preservation.

References

Angelillo, Babilio, Fortunato, 2013: Angelillo M., Babilio E., Fortunato A., “Singular stress fields for masonry-like vaults”, in *Continuum Mechanics and Thermodynamics*, 25 (2013), nn. 2-4, pp. 423-441; DOI: 10.1007/s00161-012-0270-9.

Angelillo, Olivieri, DeJong, 2021: Angelillo M., Olivieri C., DeJong M.J., “A new equilibrium solution for masonry spiral stairs”, in *Engineering Structures*, 238 (2021), April, article number 112176; DOI: 10.1016/j.engstruct.2021.112176.

Baratta, Corbi, 2010: Baratta A., Corbi O., “On the equilibrium and admissibility coupling in NT vaults of general shape”, in *International Journal of Solids and Structures*, 47 (2010), n. 17, pp. 2276-2284; DOI: 10.1016/j.ijsolstr.2010.04.024.

Block, Ochsendorf, 2007: Block P., Ochsendorf J., “Thrust network analysis: A new methodology for 3D equilibrium”, in *Journal of the International Association for Shell and Spatial Structures*, 48 (2007), n. 155, pp. 1-7.

Block, 2009: Block P., *Thrust Network Analysis: Exploring Three-dimensional Equilibrium*, Massachusetts Institute of Technology, 2009.

Block, Lachauer, 2014: Block P., Lachauer L., “Three-dimensional funicular analysis of masonry vaults”, in *Mechanics Research Communications*, 56 (2014), pp. 53-60; DOI: 10.1016/j.mechrescom.2013.11.010.

Block Research Group, 2021: Block Research Group, *RhinoVault2* [online]; <<https://github.com/BlockResearchGroup/compas-RV2>>, accessed on Dec. 13, 2021.

Bruggi, 2020: Bruggi M., “A constrained force density method for the funicular analysis and design of arches, domes and vaults”, in *International Journal of Solids and Structures*, 193-194 (2020), pp. 251-269; DOI: 10.1016/j.ijsolstr.2020.02.030.

Calladine, 1983: Calladine C.R., *Theory of Shell Structures*, Cambridge University Press, 1983.

Fraddosio, Lepore, Piccioni, 2020: Fraddosio A., Lepore N., Piccioni M.D., “Thrust Surface Method: An innovative approach for the three-dimensional lower bound Limit Analysis of masonry vaults”, in *Engineering Structures*, 202 (1 Jan. 2020), article number 109846; DOI: 10.1016/J.ENGSTRUCT.2019.109846.

Fraternali, Angelillo, Fortunato, 2002: Fraternali F., Angelillo M., Fortunato A., “A lumped stress method for plane elastic problems and the discrete-continuum approximation”, in *International Journal of Solids and Structures*, 39 (2002), n. 25, pp. 6211-6240; DOI: 10.1016/S0020-7683(02)00472-9.

Fraternali, 2010: Fraternali F., “A thrust network approach to the equilibrium problem of unreinforced masonry vaults via polyhedral stress functions”, in *Me-*

chanics Research Communications, 37 (2010), n. 2, pp. 198-204; DOI: 10.1016/j.mechrescom.2009.12.010.

Heyman, 1966: Heyman J., "The stone skeleton", in *International Journal of Solids and Structures*, 2 (Apr. 1966), n. 2, pp. 249-279; DOI: 10.1016/0020-7683(66)90018-7.

Heyman, 1977: Heyman J., *Equilibrium of Shell Structures*, Oxford, Clarendon Press Oxford, 1977.

Heyman, 1988: Heyman J., "Poleni's problem", in *Proceedings of the Institution of Civil Engineers*, 84 (Aug. 1988), n. 4, pp. 737-759; DOI: 10.1680/iicep.1988.139.

Heyman, 1995: Heyman J., *The stone skeleton*, Cambridge, Cambridge University Press, 1995.

Heyman, 2017: Heyman J., "The safety of masonry arches", in *Masonry Bridges, Viaducts and Aqueducts*, 11 (Nov. 1968), Routledge, 2017, pp. 329-352.

Huerta, 2001: Huerta S., "Mechanics of masonry vaults: the equilibrium approach", in *Proceedings of the 1st International Conference on Structural Analysis of Historical Constructions*, Guimaraes, 2001, January, pp. 47-70.

Huerta, 2008: Huerta S., "The Analysis of Masonry Architecture: A Historical Approach", in *Architectural Science Review*, 51 (2008), n. 4, pp. 297-328; DOI: 10.3763/asre.2008.5136.

Iannuzzo, Van Mele, Block, 2020: Iannuzzo A., Van Mele T., Block P., "Piecewise rigid displacement (PRD) method: a limit analysis-based approach to detect mechanisms and internal forces through two dual energy criteria", in *Mechanics Research Communications*, 107 (2020), article number 103557; DOI: 10.1016/j.mechrescom.2020.103557.

Iannuzzo *et al.*, 2021: Iannuzzo A., Wu Y.X., Yavuzer M.N., Cusano C., Ferrero C., "When cracks are (not) a structural concern: the case of 'Giovanni Vinciguerra' School in Anagni", in *International Journal of Masonry Research and Innovation*, 1 (2021), n. 1, p. 1; DOI: 10.1504/IJMRI.2021.10039144.

Kraft, 1988: Kraft D., "A software package for sequential quadratic programming", Tech. Rep. DFVLR-FB 88-28, Koln, Germany, German Aerospace Center - Institute for Flight Mechanics, 1988.

Limit State, RING 2021: Limit State: RING - Industry Leading Masonry Arch Analysis Software | Limit State; <<https://www.limitstate.com/ring>>, last access on 24 November 2021.

Maia Avelino *et al.*, 2021a: Maia Avelino R., Iannuzzo A., Van Mele T., Block P., "Assessing the safety of vaulted masonry structures using thrust network analysis", in *Computers & Structures*, 257 (Dec. 2021), article number 106647; DOI: 10.1016/j.compstruc.2021.106647.

Maia Avelino *et al.*, 2021b: Maia Avelino R., Iannuzzo A., Van Mele T., Block P., “Parametric Stability Analysis of Groin Vaults”, in *Applied Sciences*, 11 (Apr. 2021), n. 8, p. 3560; DOI: 10.3390/app11083560.

Maia Avelino *et al.*, 2022: Maia Avelino R., Iannuzzo A., Van Mele T., Block P., “An energy-based strategy to find internal stress states compatible with general boundary displacements in masonry structures”, in *Mechanics Research Communication*, 125 (2022), pp. 103978; DOI: 10.1016/j.mechrescom.2022.103978.

Marmo, Rosati, 2017: Marmo F., Rosati L., “Reformulation and extension of the thrust network analysis”, in *Computers & Structures*, 182 (2017), pp. 104-118; DOI: 10.1016/j.compstruc.2016.11.016.

Miki, Igarashi, Block, 2015: Miki M., Igarashi T., Block P., “Parametric self-supporting surfaces via direct computation of airy stress functions”, in *ACM Transactions on Graphics*, 34 (Jul. 2015), n. 4, pp. 1-12; DOI: 10.1145/2766888.

Milani *et al.*, 2016: Milani G., Rossi M., Calderini C., Lagomarsino S., “Tilting plane tests on a small-scale masonry cross vault: Experimental results and numerical simulations through a heterogeneous approach”, in *Engineering Structures*, 123 (2016), pp. 300-312; DOI: 10.1016/j.engstruct.2016.05.017.

Moseley, 1843: Moseley H., *On the Theory of the Arch. The Theory, Practice and Architecture of Bridges...*, editado por John Weale, London, Architectural Library, vol. I, part III, pp. 1-72, láms. 101-3, 1843.

Nodargi, Bisegna, 2021: Nodargi N.A., Bisegna P., “Collapse capacity of masonry domes under horizontal loads: A static limit analysis approach”, in *International Journal of Mechanical Sciences*, 212 (2021), pp. 106827; DOI: 10.1016/j.ijmecs-ci.2021.106827.

O’Dwyer, 1999: O’Dwyer D., “Funicular analysis of masonry vaults”, in *Computers & Structures*, 73 (1999), nn. 1-5, pp. 187-197; DOI: 10.1016/S0045-7949(98)00279-X.

Ochsendorf, 2002: Ochsendorf J., *Collapse of masonry structures*, University of Cambridge, 2002.

Poleni, 1748: Poleni G., *Memorie Istoriche della gran cupola del tempio vaticano*, Padova, nella Stamperia del Seminario, 1748.

Rippmann, Lachauer, Block, 2012: Rippmann M., Lachauer L., Block P., “Interactive Vault Design”, in *International Journal of Space Structures*, 27 (2012), n. 4, pp. 219-230; DOI: 10.1260/0266-3511.27.4.219.

Rippmann, Block, 2017: P Rippmann M., Block P., “Funicular Shell Design Exploration”, in Leach N., Yuan P.F. (eds.), *Computational Design*, Shanghai, Tongji University Press, 2017 (January).

Schek, 1974: Schek H., “The force density method for form finding and computa-

tion of general networks”, in *Computer Methods in Applied Mechanics and Engineering*, 3 (1974).

Shin *et al.*, 2016: Shin H.V., Porst C.F., Vouga E., Ochsendorf J., Durand F., “Reconciling elastic and equilibrium methods: For static analysis”, in *ACM Transactions on Graphics*, 35 (2016), n. 2; DOI: 10.1145/2835173.

Smars, 2000: Smars P., *Etudes sur la stabilité des arcs et voûtes, confrontation des méthodes de l'analyse limite aux voûtes gothiques en Brabant*, PhD thesis, K.U. Leuven, 2000.

Svanberg, 1987: Svanberg K., “The method of moving asymptotes—a new method for structural optimization”, in *International Journal for Numerical Methods in Engineering*, 24 (Feb. 1987), n. 2, pp. 359-373; DOI: 10.1002/nme.1620240207.

Tralli, Alessandri, Milani, 2014: Tralli A., Alessandri C., Milani G., “Computational Methods for Masonry Vaults: A Review of Recent Results”, in *The Open Civil Engineering Journal*, 8 (Oct. 2014), n. 1, pp. 272-287; DOI: 10.2174/1874149501408010272.

Ungewitter, 1890: Ungewitter G., *Lehrbuch der gotischen Konstruktionen. III Auflage neu bearbeitet von K. Mohrmann*, 2 voll., Leipzig, T.O. Weigel Nachfolger, 1890.

Van Mele, Block, 2014: Van Mele T., Block P., “Algebraic graph statics”, in *CAD Computer Aided Design*, 53 (2014), pp. 104-116; DOI: 10.1016/j.cad.2014.04.004.

Van Mele *et al.*, 2014: Van Mele T., Panozzo D., Sorkine-Hornung O., Block P., “Best-fit thrust network analysis: Rationalization of freeform meshes”, in *Shell Struct. Archit. Form Find. Optim.*, London, Routledge, 2014, pp. 157-169; DOI: 10.4324/9781315849270.

Van Mele *et al.*, 2017: Van Mele T. *et al.*, *COMPAS: A framework for computational research in architecture and structures*, 2017; DOI: 10.5281/zenodo.2594510.

Van Mele, 2021: Van Mele T., *Compas_tna: Implementation of Thrust Network Analysis based on COMPAS*, 2020 [online]; <https://github.com/BlockResearch-Group/compas_tna>, accessed on Dec. 13, 2021.

Wächter, Biegler, 2006: Wächter A., Biegler L.T., “On the implementation of an interior-point filter line-search algorithm for large-scale nonlinear programming”, in *Mathematical Programming*, 106 (Mar. 2006), n. 1, pp. 25-57; DOI: 10.1007/s10107-004-0559-y.

Wolfe, 1921: Wolfe W.S., *Graphical Analysis: A Text Book on Graphic Statics*, New York, McGraw-Hill Book Co., Inc., 1921.

Zessin, Lau, Ochsendorf, 2010: Zessin J., Lau W., Ochsendorf J., “Equilibrium of cracked masonry domes”, in *Proceedings of the Institution of Civil Engineers: Engineering and Computational Mechanics*, 163 (2010), n. 3, pp. 135-145; DOI: 10.1680/eacm.2010.163.3.135.

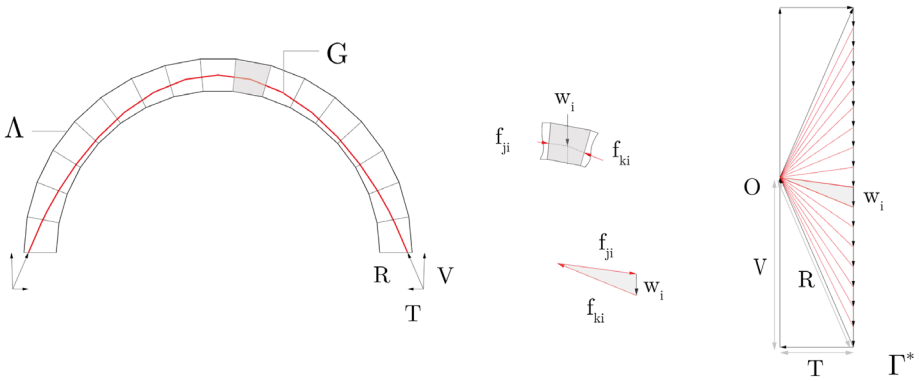


Fig. 1. Two-dimensional thrust line (G) within the semi-circular arch (Λ) highlighting the (equilibrium of) block i and reaction forces (R) with vertical (V) and horizontal (T) components. The global equilibrium is described by the force diagram (Γ^*), which is composed by the multiple local equilibria in the nodes of the thrust line's vertices.

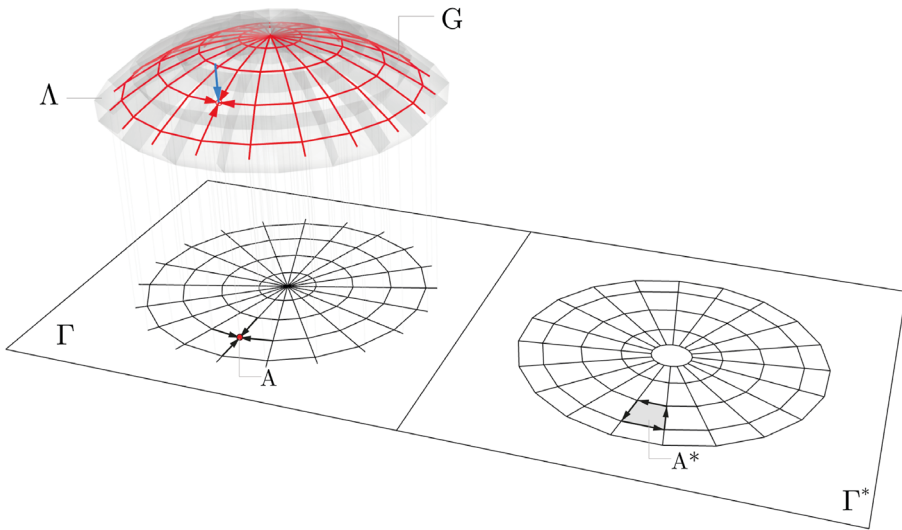


Fig. 2. A Thrust Network (G), its corresponding Form Diagram (Γ), defined as the horizontal projection of the thrusts, and the Force Diagram (Γ^*), showing the equilibrium of the forces in Γ , which are the thrusts of G . The equilibrium of the (horizontal) forces applied to the highlighted node A in Γ is represented by the closed polygon A^* in Γ^* .

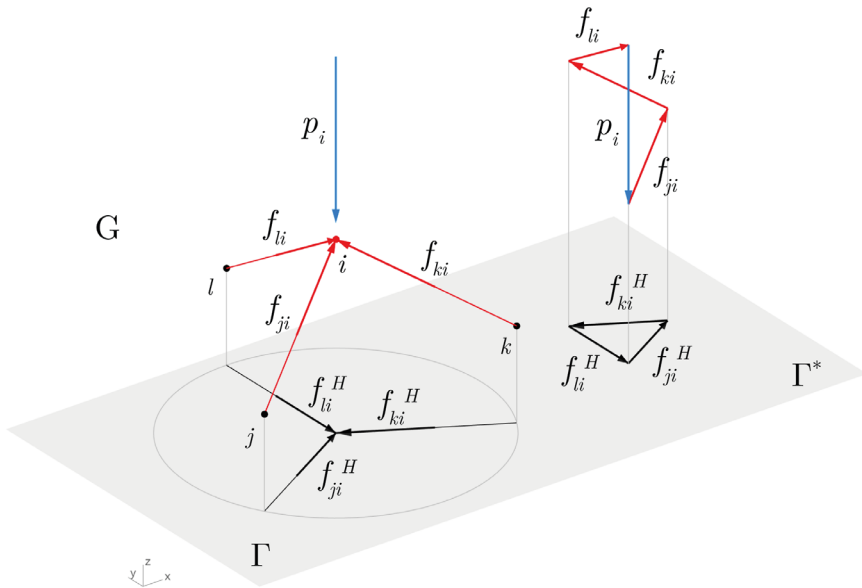


Fig. 3. Highlight of a node i in the network with an externally applied vertical load p_i . The compressive forces (f_{ji} , f_{ki} , f_{li}) in G can be decomposed in their horizontal (f_{ji}^H) and vertical (f_{ji}^V) components. The projection of the spatial equilibrium in the node results in the force diagram (Γ^*) in which the vertically applied load p_i vanishes.

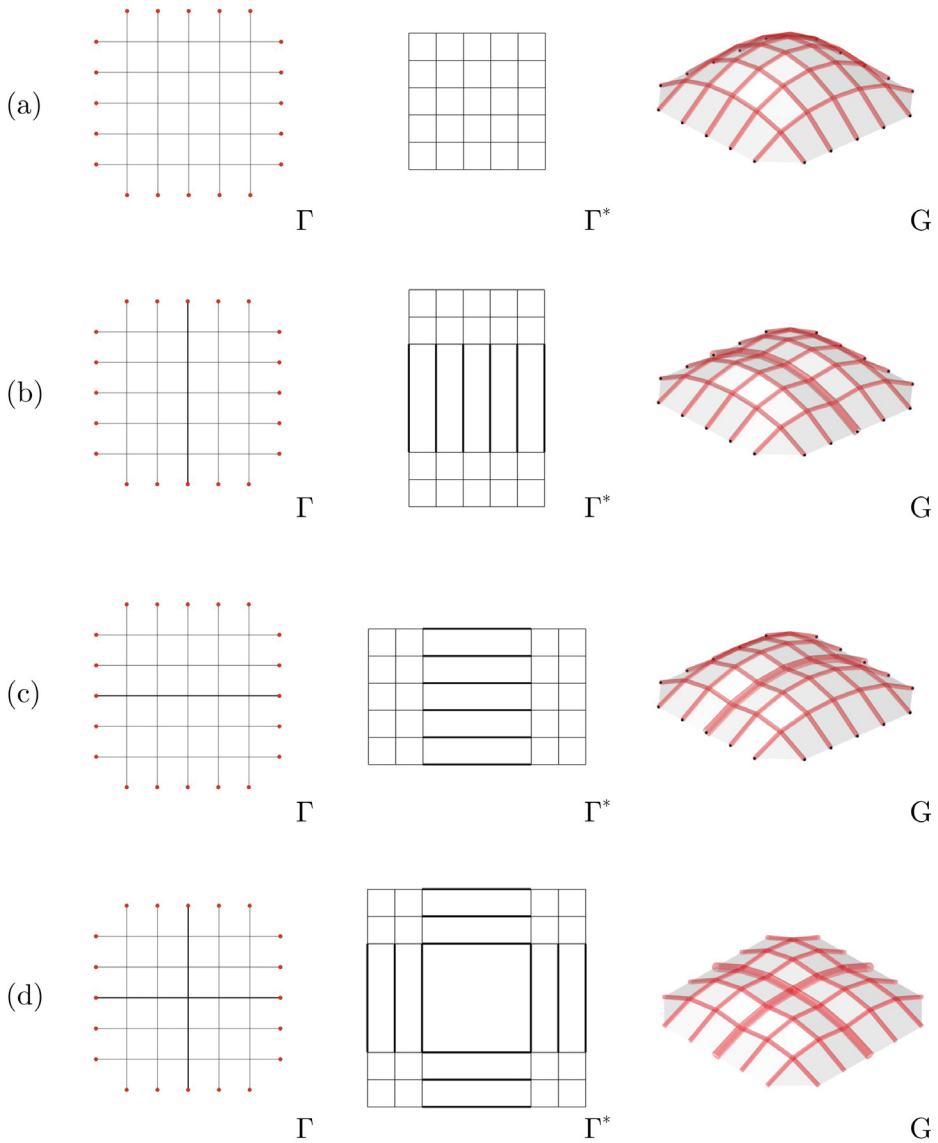


Fig. 4. Reciprocal form (Γ) and force (Γ^*) diagrams, and the resulting thrust network (G) in an orthogonal grid supported along the boundaries subjected to four different horizontal force distributions. (a) Equally distributed forces, followed by (b) forces increased in the central vertical lines of the form, (c) central, horizontal lines, and (d) central, horizontal and vertical lines. Increased horizontal forces, i.e. longer edge lengths in the force diagram, result in shallow arches, i.e. creases in the thrust networks (G). In G , the thickness of the edges are proportional to the axial force carried.

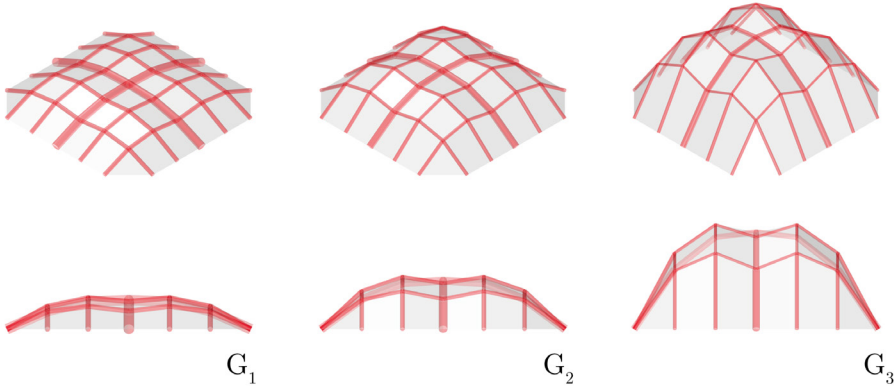


Fig. 5. Effect of the scaling factor $1/r$ in the height of the thrust network's vertices of Figure 4d. The scale factor for G is $1/r = 1$, and this factor is decreased for G_1 ($1/r_1 = 0.6$) and G_2 ($1/r_2 = 0.3$) resulting in deeper networks keeping the same horizontal distribution of the forces (i.e., the force diagram of Figure 4d).

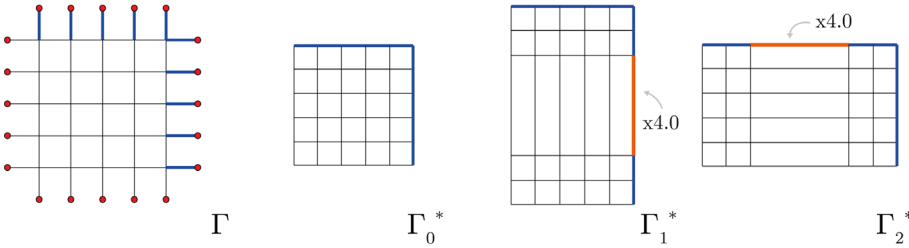


Fig. 6. Form diagram Γ with its independent edges highlighted in blue; its trivial reciprocal force diagram Γ_0^* in which the forces are equally distributed and the dual independent edges are highlighted. Two modifications are performed to Γ_0^* , multiplying the length of two independent edges by a factor of 4.0, which result in the force diagrams Γ_1^* and Γ_2^* .

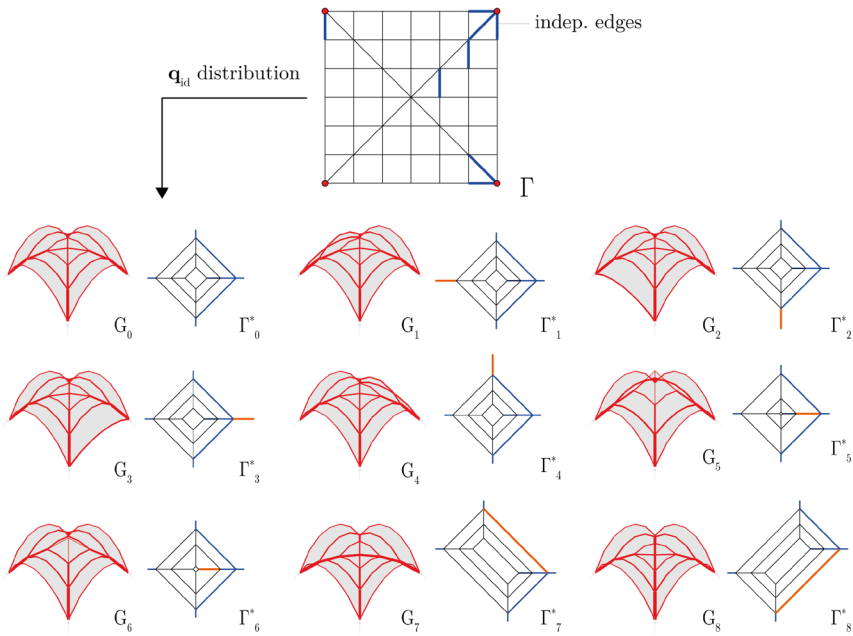


Fig. 7. Corner supported form diagram Γ with 8 independent edges (in blue). Initial force diagram Γ_0^* and thrust network G_0 , followed by an individual increase in the force of each independent edge, showing the effect in the force diagram Γ_i^* and in the thrust network G_i .

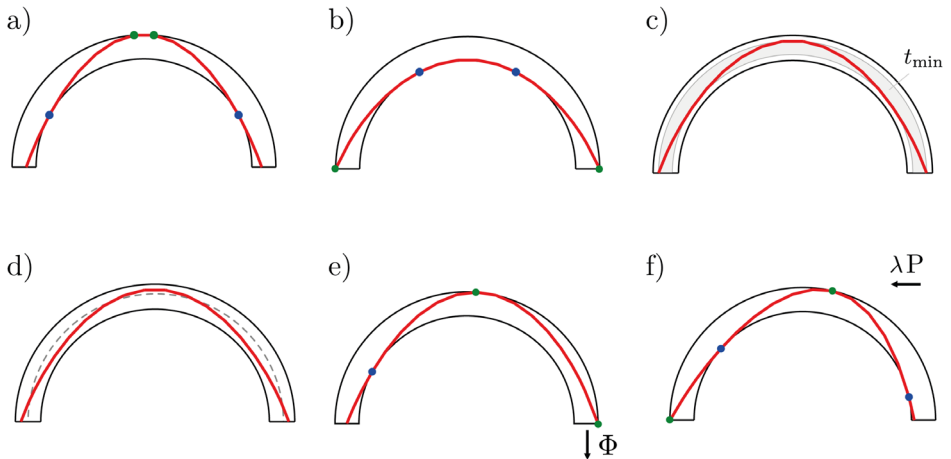


Fig. 8. Illustration on a semi-circular arch of the objective functions relevant to masonry assessment that can be explored with Thrust Network Analysis.

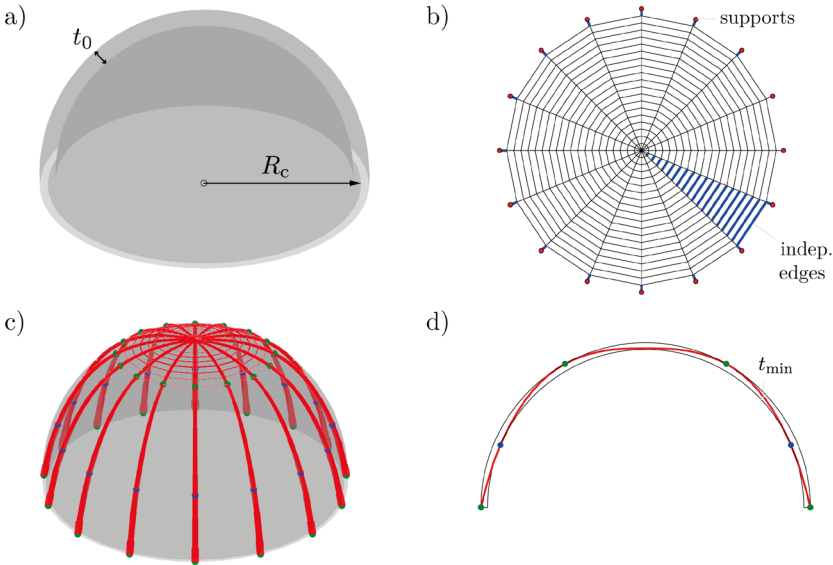


Fig. 9. (a) Perspective of the dome with initial thickness-over-radius $t_0/R_c=0.10$. (b) Form diagram used for the assessment of the hemispherical dome with support nodes in red and independent edges in blue. (c) Perspective of minimum thickness thrust network obtained with $t_{min}/R=0.041$. (d) Main cross section of the dome with highlight on points where the network touches intrados (blue) and extrados (green).

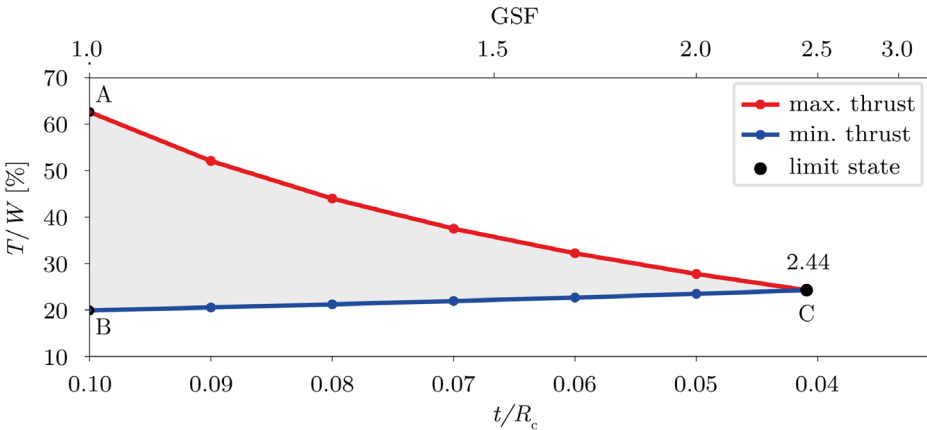


Fig. 10. Stability domain with values of normalised thrust-over-weight (T/W) for decreasing thicknesses of the dome, starting at $t_0/R_c = 0.10$. Point C highlights the limit state, corresponding to a $GSF = 2.44$. Points A and B highlight the maximum and minimum thrusts in the original state.

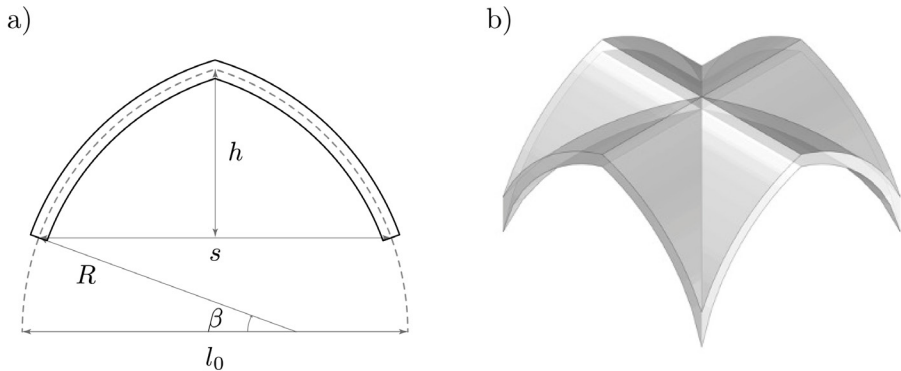


Fig. 11. (a) Parameters used to create the Gothic vaults in the study. (b) Perspective view of a Gothic vault constructed considering $R/l_0 = 0.71$, $t/s = 0.05$ and $\beta = 20^\circ$.

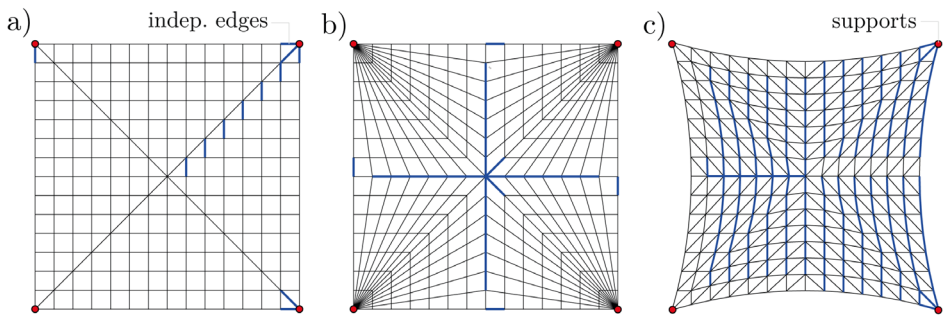


Fig. 12. Form diagrams considered for the analysis: (a) orthogonal, (b) fan-like, and (c) curved. Highlight on independent edges (blue) and supports (red).

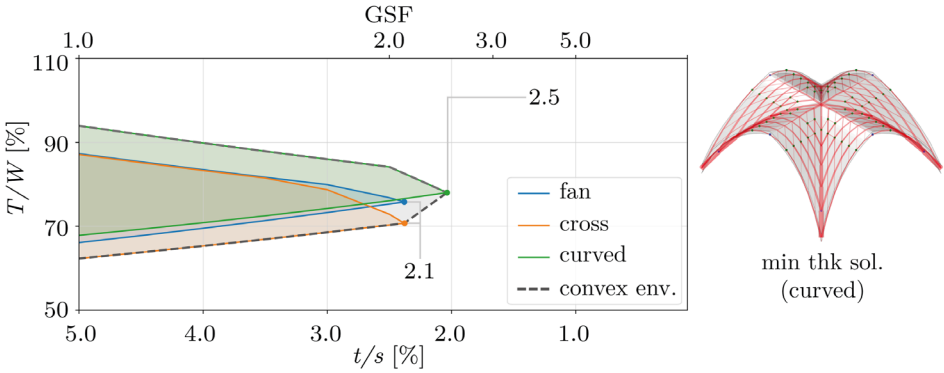


Fig. 13. Left: Stability domain for the different form diagrams in figure 12 and the convex envelope considered (grey). Right: Minimum thickness solution obtained for the curved diagram ($t_{min}/s=0.021$).

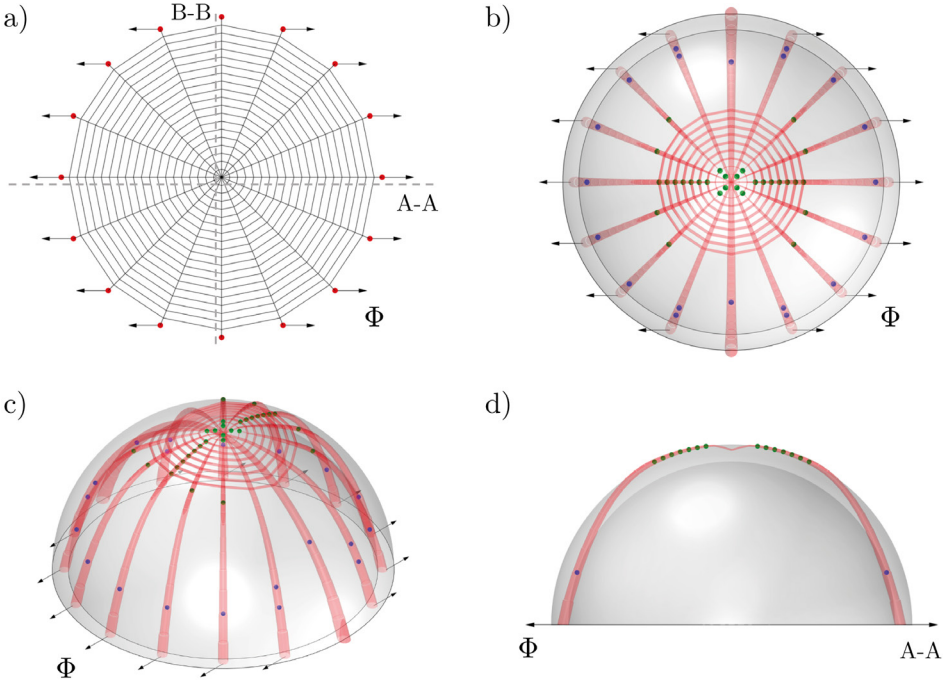


Fig. 14. (a) Assumed displacement of the supports (Φ). (b) Plan view of the found thrust network that minimises the complementary energy associated to Φ , highlighting the points where the thrust touches intrados and extrados. (c) Perspective view, and (d) sectional view of the same solution.